Surpassing Human Wrist Constraints: Dexterity-Enhanced Techniques for Teleoperated Robotic Manipulation

Luyao Shen*
Institute of Software, Chinese Academy of Sciences
Beijing, China
lshen595@connect.hkust-gz.edu.cn

Yihong Zhang
Institute of Software, Chinese Academy of Sciences
beijin, China
zhangyihong23@mails.ucas.ac.cn

Qiyuan Song
University of Michigan
AnnArbor, Michigan, USA
haoze@umich.edu

Jiannan Li
School of Computing and Information Systems
Singapore Management University
Singapore, Singapore
jiannanli@smu.edu.sg

Tianren Luo
College of Computer Science
Northwest University
Xi'an, China
luotr@nwu.edu.cn

Shuai Ma†
Institute of Software, Chinese Academy of Sciences
Beijing, China
mashuai@iscas.ac.cn

Wei Sun†
Institute of Software Chinese Academy of Sciences
Beijing, Beijing, China
sunwei2017@iscas.ac.cn

Yulong Bian
Shandong University
Weihai, Shandong, China
bianyulong@sdu.edu.cn

Jin Huang†
Institute of Software
Chinese Academy of Sciences
Beijing, China
huangjin@iscas.ac.cn

Teng Han†‡
Institute of Software, Chinese Academy of Sciences
Beijing, China
hanteng@iscas.ac.cn

Nianlong Li†§
Institute of Software, Chinese Academy of Sciences
Beijing, China
linianlong16@mails.ucas.ac.cn

Feng Tian†‡
Institute of software, Chinese Academy of Sciences
Beijing, China
tianfeng@iscas.ac.cn

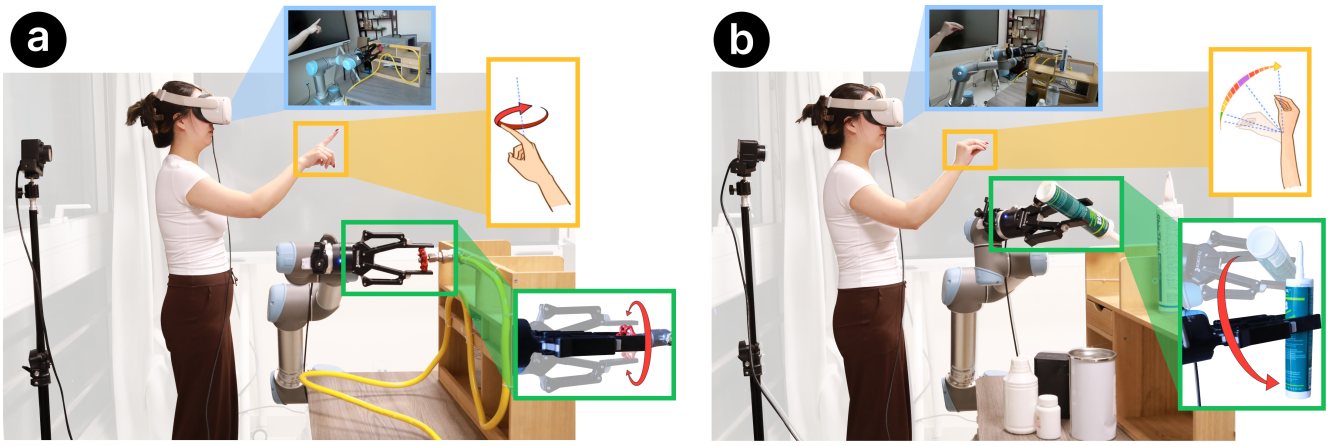


Figure 1: Enhancing robot teleoperation tasks through dexterous finger motion and non-isomorphic rotational gain: (a) gas-leak inspection, where the operator uses *FingerCircle* to close a valve and *WristDNR* to inspect potential leak points; and (b) desktop object organization, where the operator uses *WristDNR* to pick up, align, and place objects onto a shelf.

*Also with The Hong Kong University of Science and Technology (Guangzhou).
†Also with Key Laboratory of System Software (Chinese Academy of Sciences).
‡Also with School of Artificial Intelligence, University of Chinese Academy of Sciences.
§Corresponding author.

This work is licensed under a Creative Commons Attribution 4.0 International License.

UIST '26, Detroit, MI, USA

© 2026 Copyright held by the owner/author(s).

ACM ISBN 979-8-4007-2856-3/26/11
https://doi.org/10.1145/3830398.3830659

Abstract

Free-hand teleoperation enables intuitive robot control by mapping human hand and arm poses to end-effector motion. However, its effectiveness in complex tasks is constrained by the mismatch between human wrist biomechanics and robotic arm capabilities. From 60 demonstration videos across four task categories, we identified three end-effector motion capabilities that surpass human constraints: unbounded axial rotation, omnidirectional alignment, and path-constrained orientation maintenance. Inspired by enhancement techniques in virtual reality (VR), we propose two interaction strategies—*finger-based motion extension* and *non-isomorphic rotational gain*—instantiated in four methods: *FingerCircle*, *FingerRaise*, *WristSpin*, and *WristDNR*. We evaluated these methods in VR using three representative teleoperation tasks, with a clutch-based control mode as the baseline. Results showed that finger-based methods improve efficiency and agency in continuous rotation tasks, whereas wrist-based methods enhance alignment and orientation control, at the expense of predictability. We further deployed them on a UR5 robotic arm in two application scenarios. Overall, these techniques better leverage robotic dexterity while reducing operator workload.

CCS Concepts

• **Human-centered computing → Interaction techniques**.

Keywords

Teleoperation, Human–Robot Interaction, Enhanced Robot Control, Virtual Reality, Embodied Interaction

ACM Reference Format:

Luyao Shen, Yihong Zhang, Qiyuan Song, Jiannan Li, Tianren Luo, Shuai Ma, Wei Sun, Yulong Bian, Jin Huang, Teng Han, Nianlong Li, and Feng Tian. 2026. Surpassing Human Wrist Constraints: Dexterity-Enhanced Techniques for Teleoperated Robotic Manipulation. In *The 39th Annual ACM Symposium on User Interface Software and Technology (UIST '26), November 02–05, 2026, Detroit, MI, USA.* ACM, New York, NY, USA, 15 pages. https://doi.org/10.1145/3830398.3830659

1 Introduction

Teleoperation allows humans to operate robots in high-risk or inaccessible settings, such as surgery [54], space exploration [60], and disaster response [19], and is increasingly used to gather human demonstrations for training intelligent systems [51]. Recent advances in visual perception and hand tracking have made free-hand teleoperation a promising input paradigm that intuitively maps human hand movements to robot motion [11], as demonstrated by systems such as MANUS [30], Shadow Robot [49], and Plain Concepts [40] . However, its effectiveness is still limited by mismatches between human and robotic motion capabilities. High-degree-of-freedom (DoF) robotic arms provide substantial kinematic flexibility through independently rotating serial joints, supporting motions such as continuous 360° valve turning [1] and omnidirectional alignment in space docking [36]. By contrast, the human upper limb is constrained by limited rotational range and physiological joint coupling, which restrict complex maneuvers [18, 66]. This mismatch between human input and robot output reduces the fidelity of intent transfer and increases operator workload, thereby limiting teleoperation precision and the complexity of motions that can be effectively performed.

A similar challenge has been observed in virtual reality (VR), where users often operate beyond their physical range of motion (ROM). Prior work has addressed this through interaction enhancement techniques such as remapping [57] and spatial transformation [10, 12], which extend control and improve efficiency. However, these methods cannot be directly transferred to robot teleoperation. First, **the acting agent differs:** VR tasks are typically performed by the user's own hand or avatar, whereas teleoperation tasks are executed by a physical robot, placing greater demands on embodiment and collaboration experience. Second, **the physical constraints differ:** VR can support interactions beyond real world, while teleoperation must remain within the limits of physical space, robot kinematics and safety. As a result, some VR techniques, such as duplicating extra hands [48] beyond the robot's physical structure, are not applicable. Finally, **the design goals differ:** VR enhancement primarily expands human motor capability for freer and more efficient interaction, whereas teleoperation enhancement seeks to compensate for the mismatch between human input and robotic motion capability, thereby better aligning user control with the robot's operational potential. Designing effective enhancement methods for robot teleoperation under real physical constraints therefore remains underexplored and insufficiently validated.

We first reviewed 60 demonstration videos of 6-DoF robotic arms and identified three motion capabilities surpassing human wrist constraints: *unbounded axial rotation* (e.g., valve turning), *omnidirectional end-effector alignment* (e.g., assembly and docking), and *path-constrained orientation maintenance* (e.g., 3D scanning). To address human physiological limits, we drew on VR interaction research while accounting for teleoperation requirements such as embodiment and physical executability, and proposed two enhancement strategies: *finger-based extension*, which leverages index-finger dexterity to bypass wrist limitations while preserving body-driven control, and *non-isomorphic rotational gain*, which amplifies wrist control through nonlinear mappings while retaining familiar interaction patterns. We instantiated these strategies in four techniques (Figure 4): *FingerCircle* and *WristSpin* use circular finger motion and wrist-velocity-based rotational mapping, respectively, to support continuous rotation; and *FingerRaise* and *WristDNR* use finger lifting and non-isomorphic gain, respectively, to support omnidirectional alignment and path-constrained maintenance.

To evaluate these techniques in teleoperation, we first implemented a kinematically constrained robotic arm in VR and conducted a user study using clutching-based control as the baseline. The study comprised three tasks: valve rotation to compare *FingerCircle* and *WristSpin*, and object placement and buzz-wire tracking to compare *FingerRaise* and *WristDNR*. Results showed that all four enhanced techniques improved operational efficiency and reduced physical re-adjustment. Compared with *WristSpin*, *FingerCircle* increased users' sense of agency through its more synchronous finger-to-robot mapping. *FingerRaise* provided more targeted support in anatomically constrained directions, whereas *WristDNR* delivered more consistent overall gains but sometimes reduced predictability. Both *FingerRaise* and *WristDNR* also increased collisions. Overall, our results provide empirical guidance for configuring free-hand teleoperation enhancement strategies, particularly in balancing

efficiency, precision, and embodied control. By further deploying *FingerCircle* and *WristDNR* on a UR5 robotic arm in two scenarios—gas-leak inspection and desktop object organization (Figure 1), we demonstrated their practical value for flexible teleoperation through expert interviews, while also identifying challenges in hardware latency and safety-driven redundancy control.

This paper makes the following contributions: i) define three categories of end-effector motion capabilities that surpass human constraints; ii) propose two interaction strategies, instantiate as four interaction techniques; iii) evaluate them in three representative virtual teleoperation tasks and two physical-robot scenarios.

2 Related Work

We review free-hand teleoperation and strategies for extending limited 3D manipulation, including dexterous finger motions and non-isomorphic rotational techniques.

2.1 Free-hand Teleoperation

Previous research on free-hand teleoperation generally falls into two categories: discrete and continuous approaches [28]. Discrete approaches map predefined hand poses to robot actions. For example, Cabrera et al. [4] used CNN-based gesture recognition to let users operate a charging robot through a teleconferencing interface, while Xue et al. [64] defined nine gestures to trigger end-effector actions. While effective for simple tasks, these systems rely on a fixed gesture vocabulary and therefore provide limited expressiveness.

In contrast, continuous approaches support finer-grained and more responsive control by directly mapping the operator's hand and arm poses to end-effector kinematics. They have been widely used in hazardous environment teleoperation [65] and demonstration-based teaching because free-hand movement allows operators to intuitively guide end-effector motion [33, 45]. These systems typically use a two-finger gripper (e.g., [17, 33]) and begins with a predefined gesture, such as a three-finger pinch [68], to activate the robotic arm. The operator then controls translation and rotation through hand motion [8, 16], while grasping is commonly triggered by fingertip contact and separation [68] or a palm grasp [8]. Despite their higher interaction bandwidth, continuous approaches remain constrained by the operator's physical ROM [55]. When tasks require end-effector configurations near or beyond the anatomical limits of wrist or forearm rotation, operators typically rely on repeated clutching-pausing the mapping, repositioning the arm, and then resuming control [44].

2.2 Dexterous Finger Motion for Input Extension

Fingers are among the most dexterous and precise parts of the human body, supporting grasping and fine manipulation through their multiple joints and rich motion capabilities [39]. Prior work has shown that finger dexterity can enhance 3D interaction in many ways. For example, Benko and Feiner [3] mapped inter-finger distance to cursor height for efficient 3D selection. Matulic and Vogel [32] projected independent rays from each finger, enabling direct manipulations via geometric ray patterns. Even in tool-based input such as VR controllers [2, 20], styluses [26, 31], and dual-stick [27], finger movements have served as additional input channels to expand interaction.

More recently, research has shifted from whole-hand gestures to fast, eyes-free microgestures usable while holding objects [5, 50, 52] Beyond the now-common thumb–index pinch in VR [34, 38], the index finger has supported richer forms of spatial input, such as z-axis navigation [22], virtual arm control in confined VR spaces [57], and gesture drawing while holding an object [50]. These findings motivate our use of single-index-finger input to extend robotic control under constrained wrist rotation.

2.3 Non-Isomorphic 3D Rotational Techniques

Rotating 3D virtual objects is inherently challenging due to human cognitive, motor, and range-of-motion limitations [12, 15, 37]. As a result, one-to-one (isomorphic) rotation mappings between input devices and virtual objects are often inefficient, motivating the use of non-isomorphic techniques that apply static or dynamic control–display (C–D) gains to improve performance. For static gains, prior work showed that gain-scaled rotation can improve manipulation efficiency and that moderate gain values can optimize both speed and accuracy [23, 41]. For dynamic gains, PRISM adjusted the C–D ratio based on hand rotation speed to support fine control [10], and later work extended this idea to facilitate larger-angle manipulation in both 3-DOF and 6-DOF tasks [12]. Non-isomorphic rotation techniques have also been applied to viewpoint control, especially when user motion range is limited [29, 42, 43]. For example, prior studies amplified head rotation to support navigation in virtual environments and improve exploration of 360° spaces, although excessive amplification could reduce usability in head-mounted displays [42, 43]. Beyond gain-based mappings, prior work has mapped input displacement to velocity to support continuous control [9, 21, 56, 67], including viewport navigation and target selection in VR [9] and smooth end-effector motion in robot teleoperation [67]. Inspired by these studies, our work investigates whether non-isomorphic rotation techniques can enhance teleoperation performance when wrist ROM is physically constrained.

3 Interaction Design

This section identifies three motion capabilities that surpass human constraints for end-effectors and proposes two interaction strategies—leveraging dexterous finger extensions and applying non-isomorphic rotation techniques—to support them.

3.1 End-Effector Motion Capabilities Surpassing Human Constraints

To align our interaction design with the motion demands of real-world robotic manipulation, we systematically analyzed robot-arm motion patterns in teleoperation that surpass human upper-limb capabilities. Specifically, we collected 60 YouTube demonstration videos[1] spanning industrial, medical, service, and assistive applications, and grouped the identified patterns into three capabilities : *C1. Unbounded Axial Rotation (43%)*, *C2. Omnidirectional End-Effector Alignment (67%)*, and *C3. Path-Constrained Orientation Maintenance (47%)*. The percentages indicate the proportion of videos exhibiting

[1]The complete list of videos is provided in the Supplementary Material.

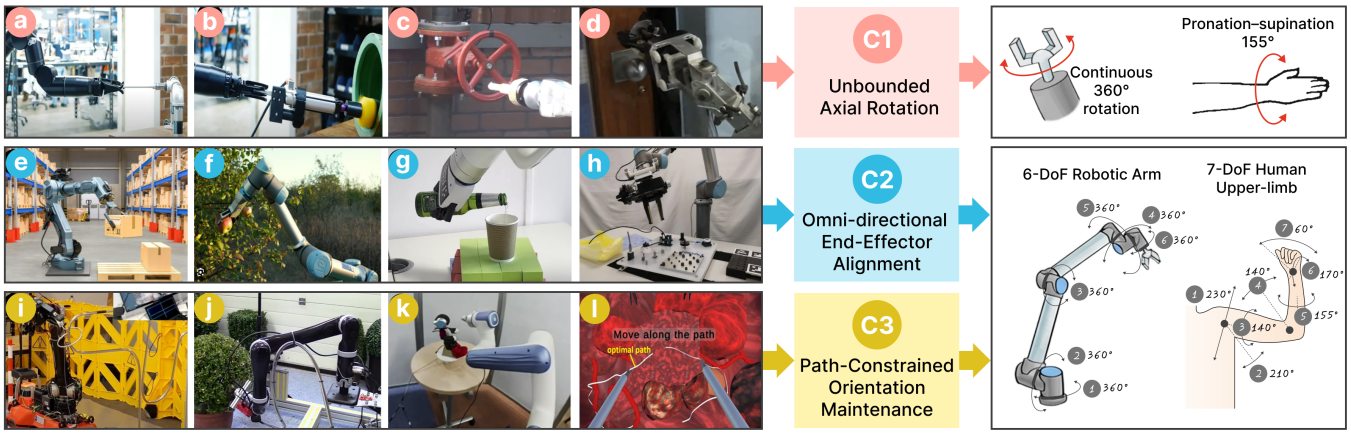


Figure 2: Identification and analysis of end-effector motion capabilities that surpass human constraints. Left: Example scenarios include (a) screwing bolts, (b) cleaning pipes, (c) turning valves, (d) turning door handles; (e) pick-and-place, (f) fruit picking, (g) pouring liquids, (h) peg-in-hole assembly; (i) buzzwire game, (j) bushes cutting, (k) 3D scanning, (l) surgical organ avoidance; Center: three motion capabilities that surpass human constraints for end-effectors; Right: Robot joints can rotate independently through 360°, while human upper-limb joints are coupled and range-limited. Human joint angle data are from [18, 66].

each capability. Drawing on biomechanics literature on human joint constraints and robotics literature on end-effector joint structures, we attributed these patterns to two underlying sources: single-joint limitations in ***C1*** and multi-joint coupling limitations in ***C2*** and ***C3***, as shown in Figure 2, which differ in whether orientation change is constrained by a movement path.

C1. Unbounded Axial Rotation. The human forearm is anatomically limited to about ±70°–85° of axial rotation by the radioulnar joint [66], a hard constraint that adjacent joints cannot compensate for. By contrast, robotic end-effectors with continuous rotation joints have no such physical constraint, enabling unbounded axial rotation [6]. In tasks requiring repeated rotations such as tightening or screwing (Figure 2.a-d), human operators must frequently reverse wrist posture or compensate with elbow and shoulder movements, whereas end-effectors can perform smooth, continuous rotations without altering overall posture.

C2. Omnidirectional End-Effector Alignment. Due to joint coupling in the human upper limb, simultaneous coordination of shoulder, elbow, and wrist is required to achieve stable end-effector alignment across arbitrary orientations. This coupling collectively constrains the reachable orientation space [18]. Robotic end-effectors with independently actuated joints are free of this coupling, enabling flexible orientation control across the global orientation space [53]. In tasks such as docking, assembly, or fruit picking (Figure 2.e-h), operators often need to repeatedly adjust body posture or rely on external fixtures. Robotic arms, however, can exploit independent DoF to accommodate multi-angle and multi-posture requirements with ease.

C3. Path-Constrained Orientation Maintenance. Simultaneously maintaining end-effector orientation while following a task-constrained path or surface imposes dual coordination demands that can degrade human performance [47], even apart from joint ROM limits. Robotic arms can decouple these requirements through motion planning algorithms [53], preserving end-effector orientation during path following. In tasks such as buzzwire, 3D scanning, or surgical avoidance (Figure 2.i–l), robotic arms can leverage redundant DoF and advanced planning to maintain orientation consistently and precisely, where human performance typically declines.

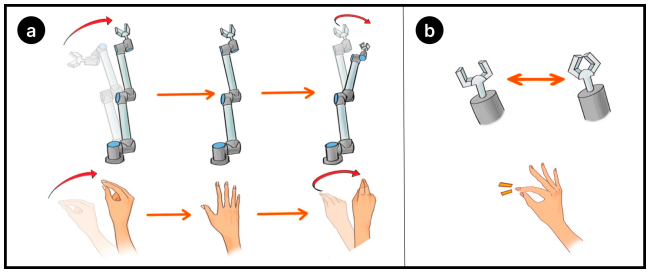


Figure 3: *Basic Control Mode.* (a) Users grab and release with a three-finger pinch, and (b) use a double-pinch to switch between picking and placing.

3.2 Basic Control (BC) Mode

Our interaction strategies build on enhancements to a basic gesture-based control mode; we therefore begin by defining this default mode of operation. Consistent with prior continuous freehand teleoperation systems, such as Zhang et al. [68] (see section 2.1), we adopt a clutching-based control scheme (Figure 3). When the operator performs a three-finger pinch gesture, the end effector enters an active control state in which its translation and rotation are directly driven by hand motion. When the gesture is released, the end effector immediately freezes, allowing the operator to reposition the hand without affecting the robot state. Gripper closing and opening are toggled via a double-pinch gesture, which is detected when the index finger's instantaneous acceleration exceeds a predefined threshold and two pinch events occur within a fixed temporal window (e.g., 500 ms).

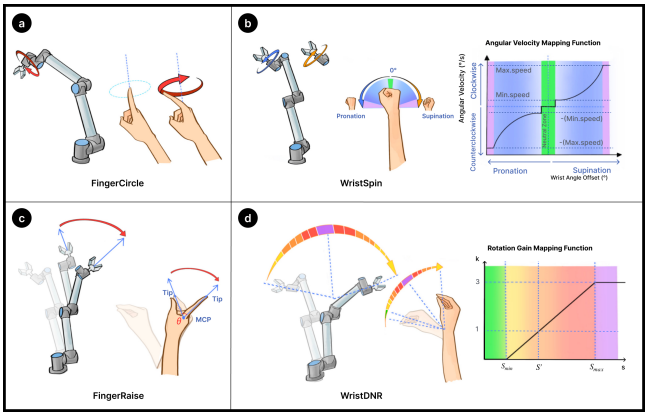


Figure 4: Four enhancement techniques: (a) *FingerCircle* and (c) *FingerRaise*, both based on index finger extension; (b) *WristSpin* and (d) *WristDNR*, both based on non-isomorphic rotational gain.

3.3 Interaction Strategy 1: Leveraging Index Finger to Extent Motion

Our first enhancement strategy leverages finger dexterity to extend the rotational limits of the wrist. This strategy is motivated by prior research [22, 32, 50], which demonstrates the index finger's superior independence and fine motor control compared to other digits, making it especially effective for precise and complex movements. Building on this insight, we introduce two index-finger-based enhancement techniques: ***FingerCircle***, which supports ***C1***, and ***FingerRaise***, which supports both ***C2*** and ***C3***.

3.3.1 FingerCircle. FingerCircle enables continuous rotation of the robot end effector through circular motion of the index finger. As shown in Fig. 4.a, when the user extends the index finger and briefly holds it still (e.g., for 200 ms), the system registers the current pointing direction as the center of rotation. The circular trajectory subsequently traced by the index finger in midair is then projected onto a plane, and the resulting angular displacement is mapped to the end effector's rotation around the tool axis, enabling smooth and continuous control. A floating circular UI visualizes the projected fingertip position to guide the motion. Retracting the index finger returns the system to the *BC* mode, while fully opening the hand immediately freezes the end-effector at its current pose.

3.3.2 FingerRaise. FingerRaise extends the effective wrist rotation range by mapping upward index-finger deflection to a rotational command (Figure 4.c). Let $\mathbf{a}, \mathbf{b} \in \mathbb{R}^3$ denote the index-finger pointing directions before and after the lifting motion. Following Matulic and Vogel [32], the pointing direction of the index finger is defined as the ray from the metacarpophalangeal (MCP) joint to the fingertip. We estimate the relative rotation that aligns $\mathbf{a}$ with $\mathbf{b}$ and represent it as a quaternion $q_{\mathbf{a}\to\mathbf{b}}$. A quaternion comprises a three-dimensional vector component encoding the rotation axis and a scalar component related to the rotation angle. We then apply this incremental rotation to update the current wrist orientation q:

$$q' = q_{\mathbf{a}\to\mathbf{b}} \otimes q, \tag{1}$$

where $\otimes$ denotes quaternion multiplication. This formulation maps index-finger lifting to wrist rotation. Full mathematical details are provided in Appendix A.1.1 and A.1.2.

FingerRaise is activated during three-finger pinch manipulation when the index finger is lifted beyond a predefined threshold (e.g., 1 cm) while the thumb and middle finger remain pinched. Lowering the index finger returns control to the *BC* mode, and releasing the thumb and middle finger terminates robotic arm control.

3.4 Interaction Strategy 2: Non-Isomorphic Rotation Gain

Our second enhancement strategy extends wrist-based control by applying a non-isomorphic rotation gain. This technique, widely adopted in three-dimensional rotation tasks [12, 23, 41], enhances efficiency and expressiveness within a limited physical ROM. Building on this idea, we introduce ***WristDNR (Dynamic Non-Isomorphic Rotation)***, which amplifies wrist rotation input so that operators can perform large-angle orientation adjustments with less effort. This approach supports ***C2*** and ***C3***, but not ***C1***, since continuous rotation beyond 360° remains constrained by wrist anatomy. To overcome this limitation, we propose ***WristSpin***, inspired by VR scrolling techniques [9, 56], which maps wrist rotation angles to end-effector rotation speed rather than absolute orientation.

3.4.1 WristSpin. WristSpin, inspired by wrist-tilt-based velocity control in VR scrolling systems [9, 56], maps wrist pronation and supination to end-effector rotational velocity. As shown in Figure 4.b, a neutral zone (e.g., ±5°) is defined around the resting wrist orientation, within which no rotation is generated. Beyond this zone, rotational velocity increases with wrist deflection and saturates near the anatomical limit.

Formally, the nonlinear mapping function is expressed as:

$$v(x) = sign(x) \cdot (V_{min} + |x|^b \cdot (V_{\max} - V_{min})), \quad b \geq 1, \tag{2}$$

where x is the wrist deflection angle normalized to $[0, 1]$, b is the gain exponent controlling the nonlinearity of the response (set to 3.3 in our study, following [56]), $V_{\max}$ and $V_{\min}$ denote the maximum and minimum rotational velocities, and $sign(x)$ indicates the direction of rotation (positive for clockwise, negative for counterclockwise). *WristSpin* is activated when the hand forms a fist within the neutral zone, and it is deactivated when the hand is fully opened.

3.4.2 WristDNR. WristDNR dynamically scales the mapping between wrist motion and end-effector rotation using a gain function $k(S)$, which is determined by wrist angular velocity S. Following prior work [10, 12], we define the nonlinear mapping function as:

$$k(S) = \frac{1}{CD} = \begin{cases} 0, & S < S_{\min}, \\ k_{\max} \cdot \frac{S - S_{\min}}{S_{\max} - S_{\min}} & S_{\min} \leq S \leq S_{\max}, \\ k_{\max}, & S > S_{\max} \end{cases} \tag{3}$$

where CD is the control-display ratio between wrist motion and end-effector motion , $S_{\min}$ and $S_{\max}$ denote velocity thresholds, and $k_{\max}$ is the maximum scaling factor (set to 1.8 in our study, following [41]). We set $S_{\max}$ to 90°/s following [12], and $S_{\min}$ to

$30^\circ/s$ based on a pilot study accounting for the greater instability of free-hand input. As shown in Figure 4.d, motions below $S_{\min}$ are suppressed to reduce noise from hand instability. The critical velocity S' separates two control ranges : when $S < S'$, rotations are attenuated ($k < 1$) for precise fine-tuning, whereas when $S > S'$, rotations are amplified ($k > 1$) for fast coarse-tuning. The scaling factor k is then applied through a quaternion update [23, 41]:

$$q'_e = q_{\text{diff}}^{k(S)} \otimes q_e, \tag{4}$$

where q_{diff} is the incremental wrist rotation and q_e is the current end-effector orientation. Quaternion exponentiation scales the represented rotation angle while preserving the rotation axis. Full derivations are provides in Appendix A.1.3. Unlike prior techniques, *WristDNR* directly replaces the *BC* mode with dynamic wrist-to-rotation scaling. Its activation and termination are identical to the *BC* mode: control is engaged with a three-finger pinch gesture and disengaged upon finger release.

4 User Study

To evaluate the proposed strategies, we conducted a user study using three representative teleoperation tasks—valve turning, object placement, and buzzer tracking—corresponding to the three motion capabilities that surpass human constraints, using *BC* mode as the baseline. We first implemented the techniques and tasks in VR, which provides a more stable, replicable, and comparable experimental setting than physical robot platform, and allows for intuitive mapping between user input and robot motion [61].

4.1 Method

4.1.1 Participants. We recruited 54 participants (24 female, 30 male; age range 19-35, $M = 23.94$, $SD = 3.99$) from a university via mailing lists and posters, and assigned them to three tasks (N=18 per task). Participants were assigned unique identifiers: P1-P18 for Task 1, P19-P36 for Task2, and P37-P54 for Task 3. Their professional backgrounds included industrial design, computer applications, and psychology. All participants reported to be right-handed. On a 7-point Likert scale, their self-reported familiarity scores were 4.27 for VR, 2.89 for robotic arms, and 2.94 for teleoperation. Each participant was rewarded with $USD20 for their participation. The studies in this work obtained ethics approval from a local university.

4.1.2 Apparatus. We used an Oculus Quest 3 headset to capture participants' hand movements and render the virtual environment while they remained standing. The software was developed in C# using Unity 3D (2022.3.51f1), together with the XR Interaction Toolkit and XR Hands, and was run on a MacBook Pro (2.6 GHz 6-Core Intel Core i7, 16 GB DDR4 memory, macOS Sonoma 14.4.1).

For robot simulation, we modeled a UR10 robotic arm, a 6-DoF serial industrial manipulator widely used in industrial settings [35, 63], equipped with a two-finger parallel gripper. The operator's gestures were mapped to robot motion through an inverse kinematics solver.

4.1.3 User Interface Settings. Across all tasks, the robotic arm was positioned about 0.2 m in front of the participant and aligned with the right arm along the central axis. Its base was 0.4 m lower in the participant's field of view to minimize self-occlusion of the workspace. Participants could move within a 1 m × 1 m area to maintain clear visibility. The robotic arm's maximum reach was about 1.6 m when fully extended. For Task 2 and 3, we applied a 2.5× mapping between hand displacement and end-effector motion to expand the effective workspace.

During warm-up, a UI panel on the participant's left allowed technique switching and beginning formal trials by pressing the "Finish" button after practice. The same panel was used during formal trials to proceed to the next trial or switch techniques.

4.2 Task 1: Manual Valve Turning

The first task required operators to rotate a valve about a single axis, either clockwise or counterclockwise, corresponding to ***C1*** and serving to evaluate *FingerCircle* and *WristSpin*.

4.2.1 Design and Process. We used a within-subjects design with three factors: ***Techniques*** (*BC*, *FingerCircle*, *WristSpin*), ***Directions*** (*Clockwise*, *Counterclockwise*), and ***Turns*** (*Few*: 1–5 turns; *Many*: 6–10 turns). The maximum and minimum rotational speeds of *WristSpin* were set to 650°/s and 5°/s, respectively, to match the fastest motion achievable with *FingerCircle*. Each condition was repeated five times, and the order of techniques was counterbalanced using a Latin square, yielding a total of 18 *Participants* × 3 *Techniques* × 2 *Directions* × 2 *Turns* × 5 repetitions = 1080 trials.

Before the experiment, participants were briefed on the task and instructed to rotate the valve as quickly and accurately as possible in the specified direction for the required number of turns. They practiced to familiarize themselves with the tasks and techniques. The same procedure was used for all subsequent tasks.

In each trial, participants used *BC* mode to move the end-effector and grasp the valve, and then rotated the valve with the assigned technique after a start prompt. A green arrow indicated the current valve orientation, a blue arrow indicated the target orientation, and numeric feedback displayed the remaining number of turns (Figure 5.a) . When the remaining turns reached zero, the indicator turned red. Over-rotation produced negative values (e.g., "-1 turn"), requiring participants to reverse the motion for correction. After completing the task, participants released the control gesture and pressed "Finish" to proceed to the next trial. Participants could rest between techniques and the study lasted approximately 40 minutes.

4.2.2 Measures. We collected both objective and subjective measures. Objective metrics included *Completion Time* (from initial grasp to final release before pressing "Finish"), *Angle Error* (the absolute difference between the final and target orientations), and *Adjustment Count* (the number of discrete grasp—rotate—release cycles). Subjective measures included *NASA-TLX* for perceived workload [14], *Sense of Agency (SoA)* for perceived control over end-effector motion [13], and perceived *Fluency*, *Trust*, and *Predictability* to assess the collaborative experience with the robot [59].

4.2.3 Results. We removed outliers that deviated more than three standard deviations from the mean (mean ± 3 SD) in each condition (83 trials, 7.7%). A Shapiro–Wilk test indicated that the data for completion time, angle error, and adjustment count were non-normally distributed and were therefore analyzed using the Aligned Rank Transform (ART) procedure [62]. We then conducted a repeated-measures ANOVA, followed by post-hoc pairwise comparisons with Bonferroni correction. The same procedure was applied across all

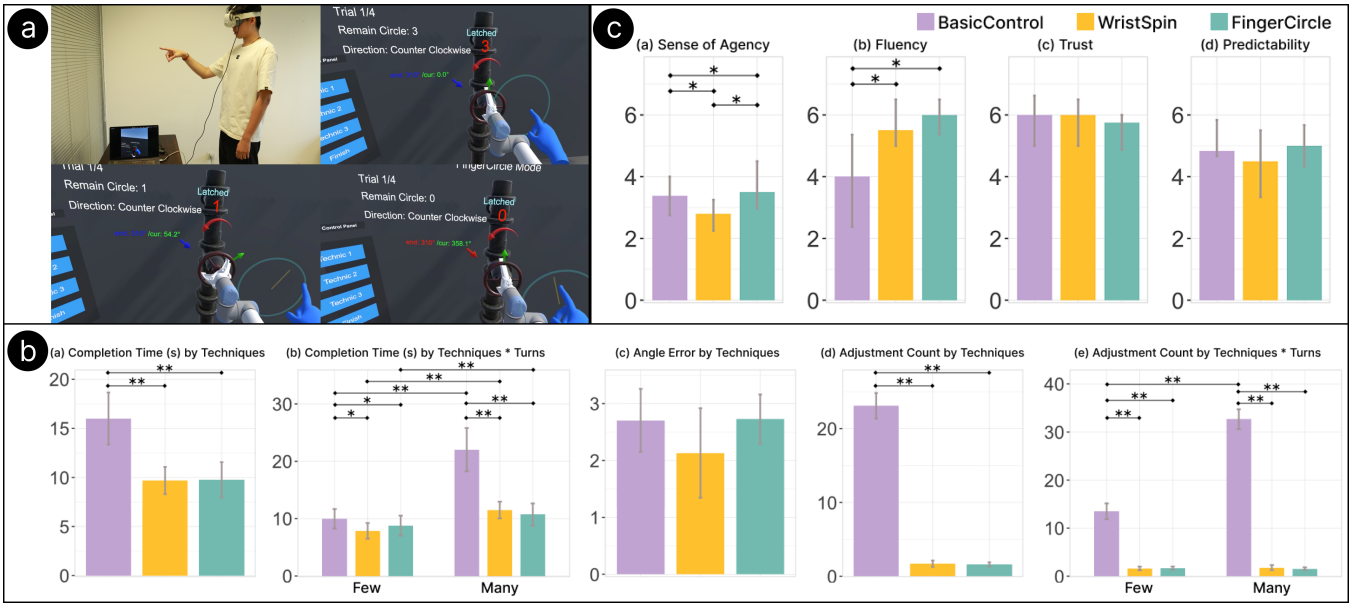


Figure 5: (a) Task 1 setup and interfaces at the beginning, during, and end of a trial; (b) Task 1 results with 95% confidence intervals error bars, and (c) *SoA*, *Fluency*, *Trust*, and *Predictability* with interquartile range error bars ($^{*}p < .05$, $^{**}p < .001$).

three tasks. Results are summarized in Figure 5.b-c and reported below:

For completion time, the analysis revealed significant main effects of *Techniques* ($F_{2,34} = 55.47, p < .001$), *Turns* ($F_{1,17} = 173.57, p < .001$), and *Techniques* × *Turns* ($F_{2,34} = 60.69, p < .001$). For adjustment count, significant main effects were also observed for *Techniques* ($F_{2,34} = 735.72, p < .001$), *Turns* ($F_{1,17} = 684.19, p < .001$), and *Techniques* × *Turns* ($F_{2,34} = 908.50, p < .001$). Pos-hoc analyses showed that both *FingerCircle* and *WristSpin* yielded significantly shorter completion times and fewer adjustments than *BC* (all $p < .05$), including under both the few-turn (all $p < .05$) and many-turn (all $p < .001$) conditions. In addition, completion time increased significantly from the few-turn to the many-turn conditions for all techniques (all $p < .001$), whereas adjustment count increased significantly only for *BC* ($p < .001$). No other effects reached statistical significance.

A Friedman test revealed significant effects of *Techniques* on *SoA* ($\chi^2(2) = 15.364, p < .001$) and *Fluency* ($\chi^2(2) = 19.770, p < .001$). Post-hoc Wilcoxon signed-rank tests with Bonferroni correction showed that *BC* yielded significantly lower *SoA* than *FingerCircle* ($Z = -2.162, p < .05$) but higher than *WristSpin* ($Z = -2.658, p < .05$). Both *FingerCircle* ($Z = -3.238, p < .05$) and *WristSpin* ($Z = -3.301, p < .05$) were rated as significantly more fluent than *BC*. For *NASA-TLX*, *Techniques* significantly affected *Mental*, *Physical Demand*, *Performance*, *Effort*, and *Frustration* (all $p < .05$); detailed results were provided in Appendix A.2.

4.2.4 Study Discussion. *FingerCircle* and *WristSpin* enabled continuous end-effector rotation through circular finger motion and wrist-velocity remapping, respectively, eliminating the frequent clutch-and-reset operations required by *BC*. Consequently, both significantly reduced completion time and adjustment count compared with *BC*, with comparable performance on both measures . Alignment accuracy was similar across all three techniques, with mean errors below 3°. Although *WristSpin* used a velocity-based mapping, its deceleration mechanism still enabled precise control near the target angle. Rotation direction also had no significant effect on performance. This may be because *FingerCircle* and *WristSpin* were symmetric by design, whereas users could compensate for the biomechanical constraints of *BC* by adjusting their initial posture. However, the mean adjustment count for both enhanced techniques remained above one, indicating that users generally still required additional fine-tuning.

The primary difference between the two enhanced techniques lay in *SoA*. Although both improved fluency and reduced physical effort, *WristSpin* significantly weakened *SoA*, even relative to *BC*. This effect likely stemmed from its angle-to-velocity mapping, which reduced the feeling of direct control. As P4 noted, *"When I was using WristSpin, I felt as if the arm was moving on its own rather than being under my direct command"*. In contrast, *FingerCircle* preserved a stronger sense of agency because finger motion remained more tightly coupled with end-effector rotation. P7 described this coupling as making *"the finger itself was an extension of the robotic arm"*, and some further characterized the interaction as "elegant" and "natural", suggesting that *FingerCircle* better balanced performance and user experience.

4.3 Task 2: Object Placement

The second task required participants to grasp an object and place it on a designated shelf. Corresponding to *C2*, this task required maintaining 3D alignment between the object and the shelf surface and was used to evaluate *FingerRaise* and *WristDNR*.

4.3.1 Design and Process. We adopted a within-subjects design with four factors: ***Techniques*** (*BC*, *FingerRaise*, *WristDNR*), shelf

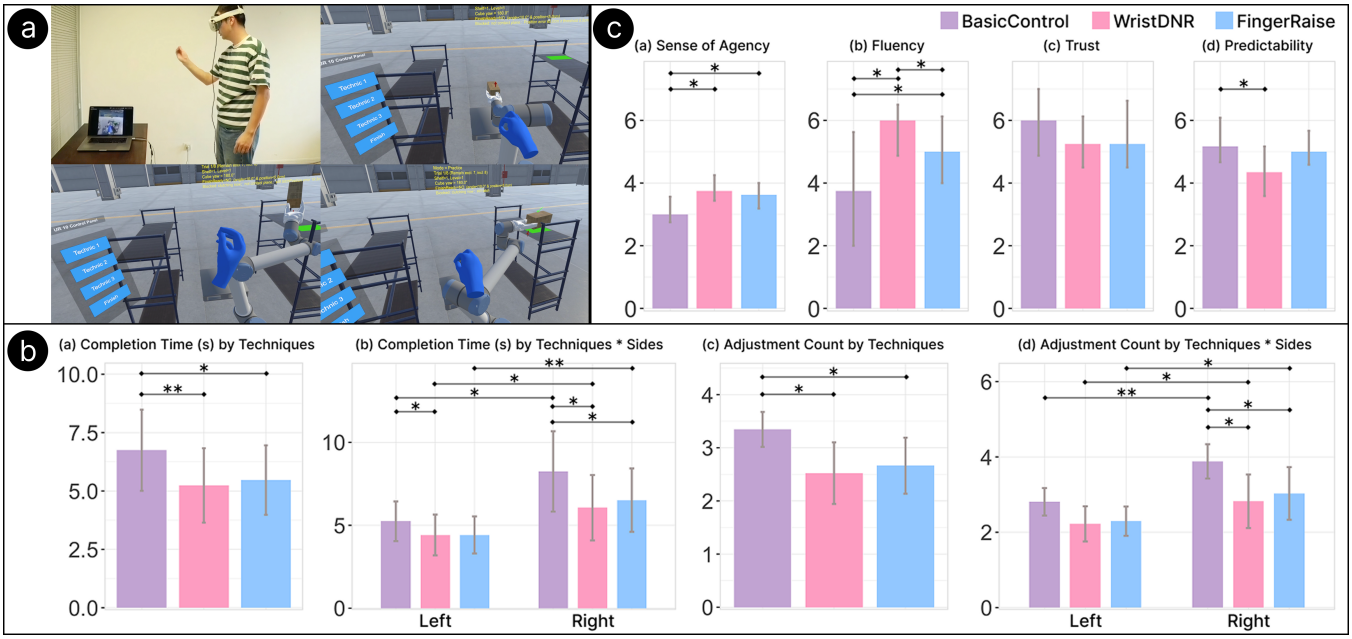


Figure 6: (a) Task 2 setup and interfaces at the beginning, during, and end of a trial; (b) Task 2 results with 95% confidence intervals error bars, and (c) *SoA*, *Fluency*, *Trust*, and *Predictability* with interquartile range error bars ($^{*}p < .05$, $^{**}p < .001$).

Sides (*Left*, *Right*), shelf ***Heights*** (*High*, *Low*), and object ***Orientations*** (*Upward*, *Downward*). Each condition was repeated five times, and the techniques order was counterbalanced using a Latin square method, yielded a total of 18 *Participants* × 3 *Techniques* × 2 *Sides* × 2 *Heights* × 2 *Orientations* × 5 repetitions = 2160 trials.

In each trial, an object (size of $20cm \times 10cm \times 10cm$) appeared 0.9 m in front of the participant, with a red arrow indicating the required placement orientation (Figure 6.a) . Participants used the assigned technique to grasp, transport, and place the object onto the green target area. The two shelves were 130 cm apart. A green checkmark appeared when the angular error was below 10° and the Euclidean distance between the object's projected center and the target was within 5 cm. Only then could participants release the object and press "Finish". Participants could rest between techniques, and the study lasted approximately 40 minutes.

4.3.2 Measures. We measured *Completion Time* and *Adjustment Count* as objective metrics, together with the subjective measures of *NASA-TLX*, *SoA*, and perceived *Fluency*, *Trust*, and *Predictability*, as described in Section 4.2.2.

4.3.3 Results. We followed the same data analysis procedure as Task 1 (Section 4.2.3), with an outlier removal rate of 4.5% (97 trials). As shown in Figure 6.b , *Completion Time* showed significant main effects of *Techniques* ($F_{2,34} = 13.35, p < .001$), *Sides* ($F_{1,17} = 22.78, p < .001$), *Orientations* ($F_{1,17} = 29.32, p < .001$), and the *Techniques* × *Sides* ($F_{2,34} = 3.65, p < .05$). *Adjustment Count* showed significant main effects of *Techniques* ($F_{2,34} = 10.067, p < .001$), *Sides* ($F_{1,17} = 23.373, p < .001$), *Orientation* ($F_{1,17} = 35.220, p < .001$), and the *Techniques* × *Sides* ($F_{2,34} = 3.547, p < .05$). Post-hoc comparisons showed that both *FingerRaise* and *WristDNR* yielded significantly faster and fewer adjustments than *BC* (all $p < .05$). In addition, right-side resulted in significantly slower (all $p < .001$) and more adjustments (all $p < .05$) than left-side across all techniques. *WristDNR* was significantly faster than *BC* on both sides (both $p < .05$), but required significantly fewer adjustments than *BC* only on right-side (both $p < .05$). *FingerRaise* was significantly faster than *BC* and required significantly fewer adjustments only on right-side ($p < .05$). No other effects reached statistical significance.

As shown in Figure 6.c , a Friedman test revealed significant effects of *Techniques* on *SoA* ($\chi^2(2) = 14.863, p < .001$), *Fluency* ($\chi^2(2) = 11.804, p < .05$), and *Predictability* ($\chi^2(2) = 6.351, p < .05$). Post-hoc Wilcoxon signed-rank tests with Bonferroni correction showed that both *FingerRaise* ($Z = -2.853, p < .05$) and *WristDNR* ($Z = -2.947, p < .05$) yielded significantly higher *SoA* ratings than *BC*. Both *FingerRaise* ($Z = -2.243, p < .05$) and *WristDNR* ($Z = -2.099, p < .05$) were also rated as significantly more fluent than *BC*, and *WristDNR* was significantly more fluent than *FingerRaise* ($Z = -2.957, p < .05$). However, *BC* was rated as significantly more predictable than *WristDNR* ($Z = -2.777, p < .05$). For *NASA-TLX*, significant effects were found for *Physical Demand* and *Effort* (both $p < .05$); detailed results were provided in Appendix A.2.

4.3.4 Study Discussion. The results showed that both *FingerRaise* and *WristDNR* outperformed *BC* by reducing completion time and grasp-reset frequency, thereby enabling more efficient object alignment. Although their overall performance was similar, their benefits varied by direction because the two techniques were differently affected by wrist motion constraints. For right-handed users, for example, *FingerRaise* primarily provided compensation when wrist motion approached its anatomical limits, yielding limited improvement over *BC* in left-side conditions but clear advantages in right-side conditions. In contrast, *WristDNR* continuously extended

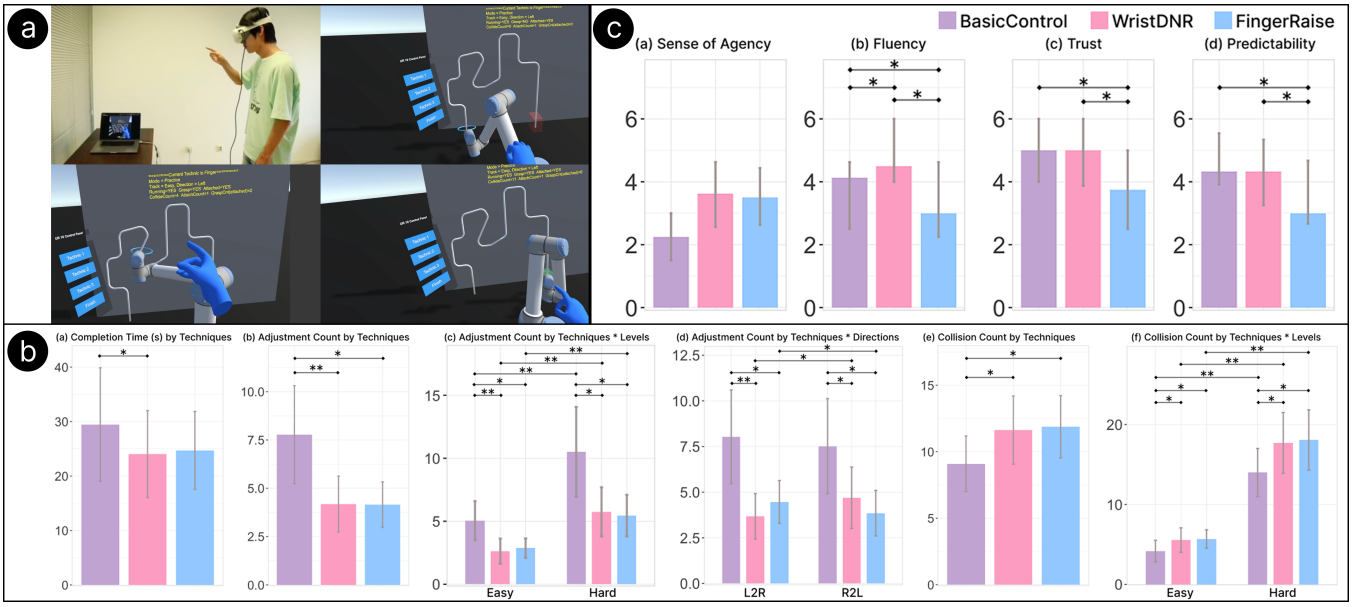


Figure 7: (a) Task 3 setup and interfaces at the beginning, during, and end of a trial; (b) Task 3 results with 95% confidence intervals error bars, and (c) *SoA*, *Fluency*, *Trust*, and *Predictability* with interquartile range error bars ($^{*}p < .05$, $^{**}p < .001$).

end-effector rotation through a non-isomorphic gain in both directions, and therefore reduced task completion time regardless of rotation direction. Because left-side operations typically remained within the wrist's natural motion range, *BC* itself did not require frequent grasp resets under that condition. Accordingly, the advantage of *FingerRaise* and *WristDNR* in reducing grasp resets was mainly observed in right-side conditions. In addition, task height had no significant effect, likely because the vertical motion range in our setup was too small to impose wrist constraints comparable to those associated with horizontal movement.

From subjective feedback, both *WristDNR* and *FingerRaise* improved *SoA* and *Fluency*. However, *WristDNR* was perceived as more fluent, likely because its gain mechanism operated continuously and implicitly, without requiring explicit activation, whereas *FingerRaise* required users to actively raise their index finger, increasing physical effort. This interpretation is consistent with the *NASA-TLX* results, in which *FingerRaise* received higher ratings for physical demand. As P30 noted, *"The advantage of FingerRaise is that the finger can finely adjust the box's placement orientation, but keeping the index finger raised for a long time becomes tiring"*. However, the implicit gain mechanism of *WristDNR* also reduced predictability: in some cases, the robot arm rotated more than users expected, making the interaction feel less direct and less predictable than *BC*.

4.4 Task 3: Buzzwire Following

The third task was a buzzwire following task in which participants guided a wire loop along a metallic obstacle without contact, which has been widely adopted in research and robotics to evaluate motor skills and precision control [25, 46]. In our study, it corresponds to *C3* and was used to evaluate *FingerRaise* and *WristDNR*.

4.4.1 Design and Process. We used a within-subject design with three factors: ***Techniques*** (*BC*, *FingerRaise*, *WristDNR*), movement ***Directions*** (*Left-to-Right (L2R)*, *Right-to-Left (R2L)*), and difficulty ***Levels*** (*Easy: 14 turns*, *Hard: 32 turns*). Each condition was repeated five times, and the order of techniques was counterbalanced using a Latin square. In total, the experiment comprised 18 *Participants* × 3 *Techniques* × 2 *Directions* × 2 *Levels* × 5 repetitions = 1,080 trials.

In each trial, a blue ring appeared at one end of the trajectory. Participants used the robotic gripper to pick up the ring, which was then replaced by the ring itself. They then employed the assigned technique to drag the ring along the trajectory toward a cube target at the opposite end, which automatically triggered the next trial upon completion (Figure 7.a). If the ring touched or left the trajectory, it turned red and an auditory "beep" signaled an error. To ensure fair comparisons, the cumulative number of collisions was displayed in the background; if it exceeded 15 on the easy track or 35 on the hard track, participants were asked to press the "Reset" button and redo the current trial. Participants could take short breaks between techniques, and the experiment lasted about 60 minutes.

4.4.2 Measures. We measured *Completion Time*, *Adjustment Count*, and *Collision Count* (the number of collisions between the ring and the trajectory) as objective metrics, together with the subjective measures of *NASA-TLX*, *SoA*, and perceived *Fluency*, *Trust*, and *Predictability*, as described in Section 4.2.2.

4.4.3 Results. We followed the same data analysis procedure as Task 1 (Section 4.2.3), with an outlier removal rate of 9.4% (101 trials). As shown in Figure 7.b , *Completion Time* showed significant main effects of *Techniques* ($F_{2,34} = 6.14, p < .05$) and *Levels* ($F_{1,17} = 44.53, p < .001$). Adjustment count showed significant main effects of *Techniques* ($F_{2,34} = 18.36, p < .001$), *Levels* ($F_{1,17} = 40.12, p < .001$), *Techniques* × *Levels* ($F_{2,34} = 9.39, p < .001$) and *Techniques* × *Directions* ($F_{2,34} = 7.56, p < .05$). Collision count

showed significant effects of *Techniques* ($F_{2,34} = 1.05, p < .001$), *Levels* ($F_{1,17} = 111.12, p < .001$), and *Techniques × Levels* ($F_{2,34} = 3.78, p < .05$).

Post-hoc comparisons revealed that both *WristDNR* and *FingerRaise* yielded significantly fewer adjustments and more collisions than *BC* (all $p < .05$), whereas only *WristDNR* was significantly faster than *BC*. Hard-level led to significantly more adjustments and collisions than easy-level across all techniques (all $p < .001$). In both the *Easy* and *Hard* conditions, *FingerRaise* and *WristDNR* required significantly fewer adjustments but produced more collisions than *BC* (all $p < .05$). For direction, we also found in both the *L2R* and *R2L* conditions, *FingerRaise* and *WristDNR* required significantly fewer adjustments than *BC* (both $p < .05$). However, *FingerRaise* required significantly fewer adjustments in *L2R* than in *R2L* direction ($p < .05$), whereas *WristDNR* showed the opposite pattern, requiring significantly fewer adjustments in *R2L* than in *L2R* ($p < .05$). No other effects reached statistical significance.

As shown in Figure 7.c , a Friedman test revealed significant effects of *Technique* on *Fluency* ($\chi^2(2) = 13.236, p < .001$), *Trust* ($\chi^2(2) = 14.292, p < .001$), and *Predictability* ($\chi^2(2) = 14.778, p < .001$). Post-hoc Wilcoxon signed-rank tests with Bonferroni correction showed that both *WristDNR* ($Z = -3.147, p < .05$) and *BC* ($Z = -2.144, p < .05$) received higher *Fluency* ratings than *FingerRaise*, and *WristDNR* was also rated higher than *BC* ($Z = -2.671, p < .05$). For both *Trust* and *Predictability*, *BC* ($Z = -2.851, p < .05$; $Z = -2.906, p < .05$) and *WristDNR* ($Z = -2.950, p < .05$; $Z = -2.676, p < .05$) were rated higher than *FingerRaise*. *NASA-TLX* results also showed significant effects on *Mental*, *Physical*, *Time Demand* , *Effort*, and *Frustration* (all $p < .05$); detailed results were provided in Appendix A.2.

4.4.4 Study Discussion. Compared with Task 2, this task required longer continuous movement, further amplifying the differences between *FingerRaise* and *WristDNR*. *FingerRaise* extended the operating range only while the index finger was raised and otherwise relied primarily on wrist motion, reducing adjustment count but not significantly shorten completion time relative to *BC*. By contrast, *WristDNR* provided continuous gain throughout the movement, reducing both completion time and adjustment count. The directional differences likely resulted from the distinct control mechanisms and asymmetric ROM. For *WristDNR*, right-handed users may rely more on forearm and elbow movements during R2L rotation, where wrist-based amplification provides limited additional benefit, leading to more adjustments. In contrast, *FingerRaise* extends the control range through finger–wrist coordination. During R2L rotation, when the wrist approached its radial-deviation limit, lifting the index finger could still provide additional control through wrist flexion. Conversely, during L2R rotation, once the wrist approached its ulnar-deviation limit, additional finger lifting provided less complementary motion due to the limited remaining wrist extension. The results also suggest a trade-off in control precision for both techniques, as reflected in increased collisions. With *BC*, users could rely on clutch-and-release to reset posture and navigate narrow regions more precisely, especially at turning points. In contrast, collisions occurred more frequently with *FingerRaise* during finger lifting and with *WristDNR* when wrist velocity was unintentionally amplified, as even small off-axis motions could be magnified.

From subjective feedback, *FingerRaise* was rated lower in *Fluency*, *Trust*, and *Predictability* because lifting the finger at the wrist's limit interrupted motion continuity. As P38 noted, *"Most of the time when I lifted my finger, the direction was not aligned with the trajectory, and the ring shifted, so I had to recalibrate."* Maintaining the index finger in a raised position also increased physical and temporal demand, as reflected in the NASA-TLX results. By contrast, *WristDNR* showed predictability comparable to *BC*. This was likely because, in the path-constrained task, participants tended to move more slowly, keeping the DNR speed gain within a controllable range.

4.5 Physical Robot Deployment

The above results suggested that, although all enhancement techniques improved task performance, their strengths differed: *FingerCircle* provided a stronger SoA, whereas *WristDNR* offered global gain enhancement and smoother movement. We therefore deployed both on a real robot platform, with users teleoperating through an Oculus Quest headset, to examine their effectiveness in more realistic scenarios (Figure 1). Using a UR5 robotic arm with a Robotiq 2F-85 parallel gripper, we designed two representative tasks: gas-leak inspection, in which operators used *FingerCircle* to close a valve, then used *WristDNR* to grasp a detector and move it along a pipeline to inspect potential leak points. This scenario combined continuous rotation and path-constrained motion, reflecting a typical teleoperation task in hazardous environments. Another was desktop object organization, in which operators used *WristDNR* to pick up scattered objects, align, and place them onto a shelf, emphasizing orientation alignment common in demonstration-based training and hazardous material handling.

We recruited six experts with prior free-hand teleoperation experience (4 male, 2 female; mean age = 30.2 years; labeled E1–E6), each of whom completed both tasks and then participated in a semi-structured interview. Overall, they found both techniques novel and engaging, and reported that they made teleoperation easier and more flexible. For example, E3 noted: *"Previously, operating the robotic arm to turn a valve felt more like manipulating a tool, but FingerCircle made it feel as if my own hand was turning the valve."* E5 stated: *"WristDNR made the process of putting these objects away much smoother, without requiring me to frequently stop and readjust my hand posture."* At the same time, physical robot deployment revealed several challenges. Delays in sensing and actuation reduced the immediacy of control, leading experts to adopt an "observe first, confirm, then continue" strategy that disrupted interaction continuity. In addition, real-world safety constraints made operators more cautious; as E2 reported, to avoid collisions, he deliberately reduced his movement amplitude and operating range, sacrificing some fluency and efficiency.

5 Discussion

5.1 Comparison and Insights of Enhancement Strategies

In this work, we proposed two enhancement strategies—finger-based extension and non-isomorphic rotational gain—and instantiated them as four interaction techniques: *FingerCircle*, *FingerRaise*, *WristSpin*, and *WristDNR*. Our results showed that all four

enhancement techniques improved teleoperation performance over *BC* mode, but through different trade-offs.

The finger-based techniques, *FingerCircle* and *FingerRaise*, improved performance while preserving a stronger sense of direct control, because end-effector motion remained more tightly coupled to users' own finger motion. This benefit was especially important for subjective experience, but it also came with limits: it required users to actively sustain finger movement, which increased fatigue during prolonged use and could interrupt fluency in continuous tasks. Moreover, although finger extension expanded the controllable range, it still remained bounded by human joint structure.

By contrast, the gain-based techniques, *WristSpin* and *WristDNR*, improved efficiency by remapping wrist motion beyond a one-to-one correspondence. Their main advantage was better support for sustained, large-range movement, where they more effectively overcame human ROM limitations. However, this came at the cost of transparency: because robot motion no longer directly matched user motion, participants sometimes reported lower *SoA* or predictability. In addition, these enhancement techniques could reduce precision; for example, *FingerRaise* and *WristDNR* were more likely to produce overshoot or collisions in fine alignment and narrow-path tasks.

Taken together, these findings suggest that enhancement in teleoperation should not be understood simply as maximizing motion amplification. Rather, it involves balancing efficiency, precision, and embodied control. Finger-based techniques appear better suited to tasks that require stronger agency and finer control, whereas gain-based techniques are more effective for large-range or repetitive movement. This points to the value of adaptive teleoperation systems that can switch between, or combine, different enhancement strategies according to task demands.

5.2 Limitations and Future Work

5.2.1 Extending to Broader Teleoperation Paradigm. This work focuses on freehand teleoperation, but teleoperation also commonly relies on controller-based interfaces, such as buttons or joysticks, to support independent control of robotic arm joints. We did not include such interfaces in our comparison, and future work should examine whether the proposed enhancement strategies generalize across different input paradigms. Our study also focuses on VR-based teleoperation, where *FingerCircle* provides a circular visual guide for fingertip motion. In non-display settings, trajectory fitting or algorithmic mapping could compensate for irregular motion. Finally, our study mainly considered robotic arms with parallel grippers. For humanoid robots with human-like morphologies, natural one-to-one mapping may suffice for general tasks such as playing tennis [69] and carrying objects [7, 24]. However, as robotic capabilities advance beyond human motion ranges and DoFs, control mismatches may re-emerge, and our enhancement strategies may inform future designs for bridging them.

5.2.2 Challenges in Physical Robot Deployment. Although we deployed our methods on a real UR5 platform, this evaluation relied mainly on expert interviews rather than a systematic quantitative study. Physical robot deployment also introduces sensing–actuation latency and more conservative operator behavior under safety constraints. These are common teleoperation challenges rather than fundamental barriers to our techniques, and recent work has begun addressing them through delay-compensation and stability-control methods, such as terminal sliding mode control with RBF neural network adaptive control [58]. In contrast, reliable bimanual hand tracking is a key prerequisite for transferring our techniques to physical robot systems. Future work should conduct systematic real-world user studies and investigate how robust hand tracking, low-latency feedback, safety awareness, and collision prediction can be integrated to better balance augmentation capability, control stability, and system safety.

5.2.3 Potential for Human Demonstration-based Robot Learning. Although this work demonstrated the value of enhanced interaction in scenarios such as gas-leak inspection and desktop object organization—covering continuous rotation, omnidirectional alignment, and path-constrained motion—these strategies may also benefit human demonstration-based robot learning. Many robot-learning methods rely on human demonstrations as training data [8, 51], yet such demonstrations are often constrained by human physiological limits rather than the robot's full mechanical capabilities. As a result, they may fail to capture the robot's full motion potential. Future work could examine whether the proposed strategies enable the collection of richer and more diverse demonstrations that better approach the robot's capability limits, and whether such data can improve robot learning and generalization.

6 Conclusion

This paper investigates how interaction enhancement can bridge the gap between human physiological limits and robot motion capabilities. We identified three motion capabilities that surpass human constraints and introduced two enhancement strategies: *finger-based motion extension* and *non-isomorphic rotational gain*, instantiated in four techniques: *FingerCircle*, *FingerRaise*, *WristSpin*, and *WristDNR*. Evaluations in both VR and on a physical robot showed that these techniques improved teleoperation efficiency and flexibility. Specifically, finger-based methods enhanced SoA in continuous rotation tasks, while wrist-based gains enabled more consistent orientation control, though sometimes at the cost of predictability. We envision future teleoperation systems could combine such strategies to better align human control with robotic affordances, supporting more effective and flexible human-robot collaboration in real-world applications.

Acknowledgments

The authors acknowledge the use of ChatGPT (OpenAI) for linguistic polishing and take full responsibility for the resulting content and the use of AI in this paper. We thank all participants in the user studies, as well as those who provided valuable feedback during the review process. This project was funded by the National Natural Science Foundation of China (62332017, T2422027) and the Beijing Natural Science Foundation (L232120).

References

[1] Seyed Reza Ahmadzadeh, Petar Kormushev, Rodrigo S Jamisola, and Darwin G Caldwell. 2014. Learning reactive robot behavior for autonomous valve turning. In *2014 IEEE-RAS International Conference on Humanoid Robots*. IEEE, 366–373.

[2] Kazuyuki Arimatsu and Hideki Mori. 2020. Evaluation of machine learning techniques for hand pose estimation on handheld device with proximity sensor.

In *Proceedings of the 2020 CHI Conference on Human Factors in Computing Systems*. 1–13.

[3] Hrvoje Benko and Steven Feiner. 2007. Balloon selection: A multi-finger technique for accurate low-fatigue 3d selection. In *2007 IEEE symposium on 3D user interfaces*. IEEE.

[4] Miguel Altamirano Cabrera, Viktor Rakhmatulin, Aleksey Fedoseev, Oleg Sautenkov, Oussama Alyounes, Andrei Puchkov, and Dzmitry Tsetserukou. 2024. OmniCharger: CNN-Based Hand Gesture Interface to Operate an Electric Car Charging Robot through Teleconference. *J. Hum.-Robot Interact.* 13, 3, Article 33 (Sept. 2024), 18 pages. doi:10.1145/3659060

[5] Adrien Chaffangeon Caillet, Alix Goguey, and Laurence Nigay. 2023. μglyph: a microgesture notation. In *Proceedings of the 2023 CHI Conference on Human Factors in Computing Systems*. 1–28.

[6] John J Craig. 2009. *Introduction to robotics: mechanics and control, 3/E*. Pearson Education India. https://www.changjiangcai.com/files/text-books/Introduction-to-Robotics-3rd-edition.pdf

[7] Yushi Du, Yixuan Li, Baoxiong Jia, Yutang Lin, Pei Zhou, Wei Liang, Yanchao Yang, and Siyuan Huang. 2025. Learning Human-Humanoid Coordination for Collaborative Object Carrying. arXiv:2510.14293 [cs.RO] https://arxiv.org/abs/2510.14293

[8] Kangkang Duan, Zhengbo Zou, and T. Y. Yang. 2025. Training of construction robots using imitation learning and environmental rewards. *Computer-Aided Civil and Infrastructure Engineering* 40, 9 (2025), 1150–1165. doi:10.1111/mice.13394

[9] Jacqui Fashimpaur, Amy Karlson, Tanya R Jonker, Hrvoje Benko, and Aakar Gupta. 2023. Investigating wrist deflection scrolling techniques for extended reality. In *Proceedings of the 2023 CHI Conference on Human Factors in Computing Systems*. 1–16.

[10] Scott Frees, G Drew Kessler, and Edwin Kay. 2007. PRISM interaction for enhancing control in immersive virtual environments. *ACM Transactions on Computer-Human Interaction (TOCHI)* 14, 1 (2007), 2–es.

[11] Qing Gao, Jinyang Li, Yimin Zhu, Siyue Wang, Jingshu Liufu, and Jinguo Liu. 2023. Hand gesture teleoperation for dexterous manipulators in space station by using monocular hand motion capture. *Acta Astronautica* 204 (2023), 630–639.

[12] Zihan Gao, Huiqiang Wang, Hongwu Lv, Moshu Wang, and Yifan Qi. 2020. Evaluating the effects of non-isomorphic rotation on 3d manipulation tasks in mixed reality simulation. *IEEE Transactions on Visualization and Computer Graphics* 28, 2 (2020), 1261–1273.

[13] Mar Gonzalez-Franco and Tabitha C Peck. 2018. Avatar embodiment. towards a standardized questionnaire. *Frontiers in Robotics and AI* 5 (2018), 74.

[14] Sandra G Hart. 2006. NASA-task load index (NASA-TLX); 20 years later. In *Proceedings of the human factors and ergonomics society annual meeting*, Vol. 50. Sage publications Sage CA: Los Angeles, CA, 904–908.

[15] Ken Hinckley, Joe Tullio, Randy Pausch, Dennis Proffitt, and Neal Kassell. 1997. Usability analysis of 3D rotation techniques. In *Proceedings of the 10th annual ACM symposium on User interface software and technology*. 1–10.

[16] Inmo Jang, Hanlin Niu, Emily C. Collins, Andrew Weightman, Joaquin Carrasco, and Barry Lennox. 2021. Virtual Kinesthetic Teaching for Bimanual Telemanipulation. In *2021 IEEE/SICE International Symposium on System Integration (SII)*. 120–125. doi:10.1109/IEEECONF49454.2021.9382763

[17] Abhishek Jha, Shital S. Chiddarwar, Rohini Y. Bhute, Veer Alakshendra, Gajanan Nikhade, and Priya M. Khandekar. 2017. Imitation Learning in Industrial Robots: A Kinematics based Trajectory Generation Framework. In *Proceedings of the 2017 3rd International Conference on Advances in Robotics* (New Delhi, India) *(AIR '17)*. Association for Computing Machinery, New York, NY, USA, Article 15, 6 pages. doi:10.1145/3132446.3134879

[18] Ibrahim A Kapandji. 1982. *The physiology of the joints, volume I, upper limb (Fifth Edition)*. Churchill Livingstone. https://graphics.cs.cmu.edu/nsp/course/16899-s16/papers/Kapandji.pdf

[19] Kapil D. Katyal, Christopher Y. Brown, Steven A. Hechtman, Matthew P. Para, Timothy G. McGee, Kevin C. Wolfe, Ryan J. Murphy, Michael D.M. Kutzer, Edward W. Tunstel, Michael P. McLoughlin, and Matthew S. Johannes. 2014. Approaches to robotic teleoperation in a disaster scenario: From supervised autonomy to direct control. In *2014 IEEE/RSJ International Conference on Intelligent Robots and Systems*. 1874–1881. doi:10.1109/IROS.2014.6942809

[20] Daehwa Kim, Keunwoo Park, and Geehyuk Lee. 2021. Atatouch: Robust finger pinch detection for a vr controller using rf return loss. In *Proceedings of the 2021 CHI Conference on Human Factors in Computing Systems*. 1–9.

[21] Won Kim, F. Tendick, S. Ellis, and L. Stark. 1987. A comparison of position and rate control for telemanipulations with consideration of manipulator system dynamics. *IEEE Journal on Robotics and Automation* 3, 5 (1987), 426–436. doi:10.1109/JRA.1987.1087117

[22] YoungIn Kim, Yohan Yun, Taejun Kim, and Geehyuk Lee. 2025. Over the Mouse: Navigating across the GUI with Finger-Lifting Operation Mouse. In *Proceedings of the 2025 CHI Conference on Human Factors in Computing Systems*. 1–14.

[23] Joseph J Laviola and Michael Katzourin. 2007. An exploration of non-isomorphic 3D rotation in surround screen virtual environments. In *2007 IEEE symposium on 3D user interfaces*. IEEE.

[24] DaeHo Lee, Ryo Suzuki, and Jin-Hyuk Hong. 2026. HumanoidTurk: Expanding VR Haptics with Humanoids for Driving Simulations. In *Proceedings of the 2026 CHI Conference on Human Factors in Computing Systems (CHI '26)*. Association for Computing Machinery, New York, NY, USA, Article 1253, 14 pages. doi:10.1145/3772318.3790397

[25] Peter Q Lee, Vidyasagar Rajendran, and Katja Mombaur. 2022. Optimization-based motion generation for buzzwire tasks with the REEM-C humanoid robot. *Frontiers in Robotics and AI* 9 (2022), 898890.

[26] Nianlong Li, Teng Han, Feng Tian, Jin Huang, Minghui Sun, Pourang Irani, and Jason Alexander. 2020. Get a grip: Evaluating grip gestures for vr input using a lightweight pen. In *Proceedings of the 2020 CHI Conference on Human Factors in Computing Systems*. 1–13.

[27] Nianlong Li, Tong Wu, Zhenxuan He, Luyao Shen, Tianren Luo, Teng Han, BoYu Gao, Yu Zhang, Liuxin Zhang, Feng Tian, et al. 2025. A Dual-Stick Controller for Enhancing Raycasting Interactions with Virtual Objects. In *2025 IEEE Conference Virtual Reality and 3D User Interfaces (VR)*. IEEE, 381–391.

[28] Rui Li, Hongyu Wang, and Zhenyu Liu. 2022. Survey on Mapping Human Hand Motion to Robotic Hands for Teleoperation. *IEEE Transactions on Circuits and Systems for Video Technology* 32, 5 (2022), 2647–2665. doi:10.1109/TCSVT.2021.3057992

[29] Tianren Luo, Tong Wu, Chaoyong Jiang, Xinran Duan, Jiafu Lv, Nianlong Li, Yachun Fan, Teng Han, and Feng Tian. 2025. RemapVR: An Immersive Authoring Tool for Rapid Prototyping of Remapped Interaction in VR. In *Proceedings of the 2025 CHI Conference on Human Factors in Computing Systems*. 1–17.

[30] MANUS. 2026. *High Precision Hand Tracking for Dexterous Manipulation.* https://www.manus-meta.com/robotics? Accessed July 12, 2026.

[31] Fabrice Matulic, Riku Arakawa, Brian Vogel, and Daniel Vogel. 2020. Pensight: Enhanced interaction with a pen-top camera. In *Proceedings of the 2020 CHI conference on human factors in computing systems*. 1–14.

[32] Fabrice Matulic and Daniel Vogel. 2018. Multiray: multi-finger raycasting for large displays. In *Proceedings of the 2018 CHI Conference on Human Factors in Computing Systems*. 1–13.

[33] Lingxiao Meng, Jiangshan Liu, Wei Chai, Jiankun Wang, and Max Q.-H. Meng. 2023. Virtual Reality Based Robot Teleoperation via Human-Scene Interaction. *Procedia Computer Science* 226 (2023), 141–148. doi:10.1016/j.procs.2023.10.648 Proceedings of International Conference on Biomimetic Intelligence and Robotics.

[34] Aunnoy K Mutasim, Anil Ufuk Batmaz, and Wolfgang Stuerzlinger. 2021. Pinch, click, or dwell: Comparing different selection techniques for eye-gaze-based pointing in virtual reality. In *Acm symposium on eye tracking research and applications*. 1–7.

[35] Abdeldjallil Naceri, Dario Mazzanti, Joao Bimbo, Yonas T Tefera, Domenico Prattichizzo, Darwin G Caldwell, Leonardo S Mattos, and Nikhil Deshpande. 2021. The vicarios virtual reality interface for remote robotic teleoperation: Teleporting for intuitive tele-manipulation. *Journal of Intelligent & Robotic Systems* 101, 4 (2021), 80.

[36] In-Won Park, Trey Smith, Hugo Sanchez, Sze Wun Wong, Pedro Piacenza, and Matei Ciocarlie. 2017. Developing a 3-DOF compliant perching arm for a free-flying robot on the International Space Station. In *2017 IEEE International Conference on Advanced Intelligent Mechatronics (AIM)*. IEEE, 1135–1141.

[37] Lawrence M Parsons. 1995. Inability to reason about an object's orientation using an axis and angle of rotation. *Journal of experimental psychology: Human perception and performance* 21, 6 (1995), 1259.

[38] Ken Pfeuffer, Benedikt Mayer, Diako Mardanbegi, and Hans Gellersen. 2017. Gaze+ pinch interaction in virtual reality. In *Proceedings of the 5th symposium on spatial user interaction*. 99–108.

[39] Roberto Francesco Pitzalis, Daegeun Park, Darwin G Caldwell, Giovanni Berselli, and Jesus Ortiz. 2023. State of the art in wearable wrist exoskeletons part i: Background needs and design requirements. *Machines* 11, 4 (2023), 458.

[40] Plain Concepts. 2026. *MRLink: Robot Teleoperation for Complex Manipulation Tasks Through Virtual Reality.* https://www.plainconcepts.com/mrlink-robot-teleoperation-virtual-reality/? Accessed July 12, 2026.

[41] Ivan Poupyrev, Suzanne Weghorst, and Sidney Fels. 2000. Non-isomorphic 3D rotational techniques. In *Proceedings of the SIGCHI conference on Human Factors in Computing Systems*. 540–547.

[42] Ivan Poupyrev, Suzanne Weghorst, Takahiro Otsuka, and Tadao Ichikawa. 1999. Amplifying spatial rotations in 3D interfaces. In *CHI'99 Extended Abstracts on Human Factors in Computing Systems*. 256–257.

[43] Eric D Ragan, Siroberto Scerbo, Felipe Bacim, and Doug A Bowman. 2016. Amplified head rotation in virtual reality and the effects on 3d search, training transfer, and spatial orientation. *IEEE transactions on visualization and computer graphics* 23, 8 (2016), 1880–1895.

[44] Daniel Rakita, Bilge Mutlu, and Michael Gleicher. 2017. A Motion Retargeting Method for Effective Mimicry-based Teleoperation of Robot Arms. In *Proceedings of the 2017 ACM/IEEE International Conference on Human-Robot Interaction* (Vienna, Austria) *(HRI '17)*. Association for Computing Machinery, New York, NY, USA, 361–370. doi:10.1145/2909824.3020254

[45] Andoni Rivera-Pinto, Johan Kildal, and Elena Lazkano. 2024. Toward Programming a Collaborative Robot by Interacting with Its Digital Twin in a Mixed Reality

Environment. *International Journal of Human–Computer Interaction* 40, 17 (2024), 4745–4757. doi:10.1080/10447318.2023.2221599

[46] Robotic Systems Lab, Legged Robotics at ETH Zürich. 2024. *AIRA Challenge: Teleoperated Mobile Manipulation for Industrial Inspection.* https://www.youtube.com/watch?v=LLD3BFS-qms YouTube video, accessed August 21, 2025.

[47] Marina Saraiva, João Paulo Vilas-Boas, Joel Marouvo, and Maria António Castro. 2022. The effect of the motor dual-task on static and dynamic postural control and classification of the motor task difficulty-Systematic Review. *Retos* 46 (2022), 264–274.

[48] Jonas Schjerlund, Kasper Hornbæk, and Joanna Bergström. 2021. Ninja hands: Using many hands to improve target selection in vr. In *Proceedings of the 2021 CHI conference on human factors in computing systems*. 1–14.

[49] Shadow Robot. 2026. *Teleoperation System—Extend your reach with intuitive remote operation across the room, or across continents!* https://shadowrobot.com/teleoperation/? Accessed July 12, 2026.

[50] Adwait Sharma, Joan Sol Roo, and Jürgen Steimle. 2019. Grasping microgestures: Eliciting single-hand microgestures for handheld objects. In *Proceedings of the 2019 CHI Conference on Human Factors in Computing Systems*. 1–13.

[51] Weiyong Si, Ning Wang, and Chenguang Yang. 2021. A review on manipulation skill acquisition through teleoperation-based learning from demonstration. *Cognitive Computation and Systems* 3, 1 (2021), 1–16. doi:10.1049/ccs2.12005

[52] Mohamed Soliman, Franziska Mueller, Lena Hegemann, Joan Sol Roo, Christian Theobalt, and Jürgen Steimle. 2018. Fingerinput: Capturing expressive single-hand thumb-to-finger microgestures. In *Proceedings of the 2018 ACM International Conference on Interactive Surfaces and Spaces*. 177–187.

[53] Mark W Spong, Seth Hutchinson, and Mathukumalli Vidyasagar. 2020. *Robot modeling and control*. Vol. 2. Wiley New York.

[54] Joseph R Sterbis, Eric J Hanly, Barry C Herman, Michael R Marohn, Timothy J Broderick, Samuel P Shih, Brett Harnett, Charles Doarn, and Noah S Schenkman. 2008. Transcontinental telesurgical nephrectomy using the da Vinci robot in a porcine model. *Urology* 71, 5 (2008), 971–973.

[55] Gilbert Tang and Phil Webb. 2018. The Design and Evaluation of an Ergonomic Contactless Gesture Control System for Industrial Robots. *Journal of Robotics* 2018, 1 (2018), 9791286. doi:10.1155/2018/9791286

[56] Theophanis Tsandilas, Emmanuel Dubois, and Mathieu Raynal. 2013. Modeless pointing with low-precision wrist movements. In *IFIP Conference on Human-Computer Interaction*. Springer, 494–511.

[57] Wen-Jie Tseng, Samuel Huron, Eric Lecolinet, and Jan Gugenheimer. 2023. Fingermapper: Mapping finger motions onto virtual arms to enable safe virtual reality interaction in confined spaces. In *Proceedings of the 2023 CHI Conference on Human Factors in Computing Systems*. 1–14.

[58] Jingwen Wang, Jiawei Tian, Xia Zhang, Bo Yang, Shan Liu, Lirong Yin, and Wenfeng Zheng. 2022. Control of time delay force feedback teleoperation system with finite time convergence. *Frontiers in Neurorobotics* 16 (2022), 877069.

[59] Yeping Wang, Pragathi Praveena, and Michael Gleicher. 2024. A design space of control coordinate systems in telemanipulation. *IEEE Access* 12 (2024), 64150–64164.

[60] Bernhard Weber, Ribin Balachandran, Cornelia Riecke, Freek Stulp, and Martin Stelzer. 2019. Teleoperating robots from the international space station: Microgravity effects on performance with force feedback. In *2019 IEEE/RSJ International Conference on Intelligent Robots and Systems (IROS)*. IEEE, 8144–8150.

[61] David Whitney, Eric Rosen, Elizabeth Phillips, George Konidaris, and Stefanie Tellex. 2019. Comparing robot grasping teleoperation across desktop and virtual reality with ROS reality. In *Robotics research: the 18th international symposium ISRR*. Springer, 335–350.

[62] Jacob O Wobbrock, Leah Findlater, Darren Gergle, and James J Higgins. 2011. The aligned rank transform for nonparametric factorial analyses using only anova procedures. In *Proceedings of the SIGCHI conference on human factors in computing systems*. 143–146.

[63] Philipp Wu, Yide Shentu, Zhongke Yi, Xingyu Lin, and Pieter Abbeel. 2024. Gello: A general, low-cost, and intuitive teleoperation framework for robot manipulators. In *2024 IEEE/RSJ International Conference on Intelligent Robots and Systems (IROS)*. IEEE, 12156–12163.

[64] Zhao Xue, Xiaoan Chen, Ye He, Hongli Cao, and Shengli Tian. 2022. Gesture- and vision-based automatic grasping and flexible placement in teleoperation. *The International Journal of Advanced Manufacturing Technology* 122, 1 (2022), 117–132.

[65] Geng Yang, Honghao Lyu, Zhiyu Zhang, Liu Yang, Jia Deng, Siqi You, Juan Du, and Huayong Yang. 2020. Keep healthcare workers safe: application of teleoperated robot in isolation ward for COVID-19 prevention and control. *Chinese Journal of Mechanical Engineering* 33, 1 (2020), 47.

[66] Y. Youm, R.F. Dryer, K. Thambyrajah, A.E. Flatt, and B.L. Sprague. 1979. Biomechanical analyses of forearm pronation-supination and elbow flexion-extension. *Journal of Biomechanics* 12, 4 (1979), 245–255. doi:10.1016/0021-9290(79)90067-8

[67] Andy Zelenak, Clinton Peterson, Jack Thompson, and Mitch Pryor. 2015. The advantages of velocity control for reactive robot motion. In *Dynamic Systems and Control Conference*, Vol. 57267. American Society of Mechanical Engineers, V003T43A003.

[68] Wei Zhang, Hongtai Cheng, Liang Zhao, Lina Hao, Manli Tao, and Chaoqun Xiang. 2019. A gesture-based teleoperation system for compliant robot motion. *Applied Sciences* 9, 24 (2019), 5290.

[69] Zhikai Zhang, Haofei Lu, Yunrui Lian, Ziqing Chen, Yun Liu, Chenghuai Lin, Han Xue, Zicheng Zeng, Zekun Qi, Shaolin Zheng, Qing Luan, Jingbo Wang, Junliang Xing, He Wang, and Li Yi. 2026. Learning Athletic Humanoid Tennis Skills from Imperfect Human Motion Data. arXiv:2603.12686 [cs.RO] https://arxiv.org/abs/2603.12686

A Appendix

A.1 Mathematical Formulations of Interaction Techniques

A.1.1 Quaternion Definitions and Operations . A quaternion is a four-dimensional representation of a 3D rotation, consisting of a vector component $\mathbf{v}$ and a scalar component w. A **unit quaternion** representing a rotation of angle θ about the unit axis $\hat{\mathbf{u}}$ is written as

$$q = (\mathbf{v}, w) = \left(\sin\frac{\theta}{2}\hat{\mathbf{u}}, \cos\frac{\theta}{2}\right), \tag{5}$$

from which the **rotation angle** can be recovered as

$$\theta = 2\arccos(w). \tag{6}$$

The inverse of a unit quaternion, $q^{-1} = (-\mathbf{v}, w)$, represents the opposite rotation. Therefore, the relative rotation from orientation q_1 to orientation q_2 can be obtained through **quaternion multiplication** as

$$q_{\text{rel}} = q_2 \otimes q_1^{-1}. \tag{7}$$

Quaternion exponentiation preserves the rotation axis while scaling the rotation angle. For a unit quaternion representing a rotation of angle θ, its **power** is

$$q^k = \left(\sin\frac{k\theta}{2}\hat{\mathbf{u}}, \cos\frac{k\theta}{2}\right), \tag{8}$$

which produces a rotation around the same axis with an angle scaled by k.

A.1.2 Mathematical Formulations of FingerRaise. To formalize *FingerRaise*, let $\mathbf{a}, \mathbf{b} \in \mathbb{R}^3$ denote the index-finger pointing directions before and after the raising motion, respectively. We first normalize the two vectors as

$$\hat{\mathbf{a}} = \frac{\mathbf{a}}{\|\mathbf{a}\|}, \quad \hat{\mathbf{b}} = \frac{\mathbf{b}}{\|\mathbf{b}\|} \tag{9}$$

We then construct a quaternion $q_{\mathbf{a}\to\mathbf{b}}$ that rotates $\hat{\mathbf{a}}$ onto $\hat{\mathbf{b}}$. The rotation axis $\hat{\mathbf{u}}$ and rotation angle θ are obtained as:

$$\hat{\mathbf{u}} = \frac{\hat{\mathbf{a}} \times \hat{\mathbf{b}}}{|\hat{\mathbf{a}} \times \hat{\mathbf{b}}|}, \tag{10}$$

$$\theta = \arccos\left(\frac{\hat{\mathbf{a}} \cdot \hat{\mathbf{b}}}{|\hat{\mathbf{a}}||\hat{\mathbf{b}}|}\right) \tag{11}$$

The corresponding incremental rotation quaternion is

$$q_{\mathbf{a}\to\mathbf{b}} = \left(\sin\frac{\theta}{2}\,\hat{\mathbf{u}},\ \cos\frac{\theta}{2}\right) \tag{12}$$

Finally, the updated end-effector orientation is obtained by

$$q' = q_{\mathbf{a}\to\mathbf{b}} \otimes q, \tag{13}$$

where $\otimes$ denotes quaternion multiplication.

A.1.3 Mathematical Formulations of WristDNR. *WristDNR* defines a dynamic rotation scaling factor $k(S)$ as a function of wrist angular velocity S. To estimate the input angular velocity, we compute the rotational difference between the current wrist orientation q_t and the orientation q_{t-1} from 200 ms earlier:

$$q_{\text{diff}} = q_t \otimes q_{t-1}^{-1} = \left(\sin\frac{\theta}{2}\hat{\mathbf{u}}, \cos\frac{\theta}{2}\right) \tag{14}$$

The corresponding rotation angle A (in degrees) is obtained from the real component w of q_{diff}:

$$A = \theta \cdot \frac{180}{\pi} = (2 \cdot \arccos(q_{\text{diff}} \to w)) \cdot \frac{180}{\pi}, \tag{15}$$

and the angular velocity S is then calculated as A/200 ms. Using Eq. 3, we compute the scaling factor k, which is then applied to amplify or attenuate the incremental rotation. The scaled quaternion is defined as:

$$q_{\text{diff}}^k = \left(\sin\frac{k\theta}{2}\hat{\mathbf{u}}, \cos\frac{k\theta}{2}\right), \tag{16}$$

where θ and $\hat{\mathbf{u}}$ are the rotation angle and axis derived from q_{diff}. Finally, the updated end-effector orientation q'_e is obtained by multiplying the incremental quaternion with the current end-effector orientation q_e:

$$q'_e = q_{\text{diff}}^k \otimes q_e \tag{17}$$

A.2 NASA-TLX Results for Task 1, Task 2, and Task 3

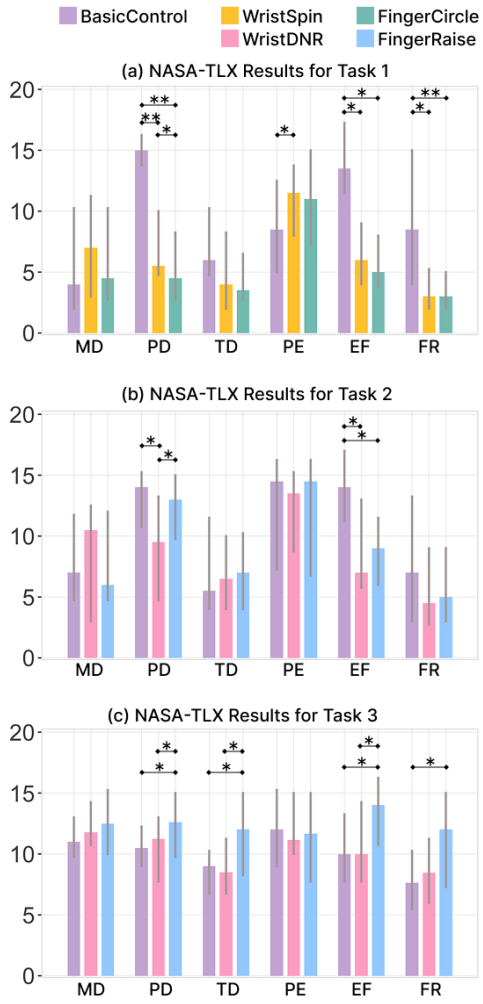


Figure 8: NASA-TLX of BC, WristSpin, WristDNR, FingerCircle, and FingerRaise in Task 1, Task 2, and Task 3, with interquartile range error bars ($^{*}p < .05$, $^{**}p < .001$).